Reliability Engineering and System Safety 228 (2022) 108804

Contents lists available at ScienceDirect

Reliability Engineering and System Safety

journal homepage: www.elsevier.com/locate/ress

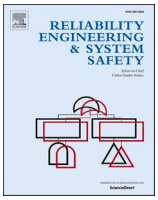

# Performance analysis of safety barriers against cascading failures in a battery pack

Lin Xie [a], Federico Ustolin [a], Mary Ann Lundteigen [a], Tian Li [b], Yiliu Liu [a,*]

[a] Norwegian University of Science and Technology, Trondheim, Norway
[b] RISE Fire Research AS, Trondheim, Norway

ARTICLE INFO

*Keywords:*
Lithium-ion battery
Reliability analysis
Cascading failure
Safety barrier

ABSTRACT

Lithium-ion batteries have been widely employed as the principal power source in electric vehicles and other storage systems. However, some critical issues in a battery pack still exist, such as thermal failures on initial cells that impact the temperatures of the surrounding cells. Such cascading failures may significantly affect battery performance and safety. Thermal barriers, as one kind of safety barrier, are therefore installed to prevent failure propagations. This paper focuses on the situation when the temperature of battery cell increases, but the battery pack still can be used in a degradation mode since the barriers are against cascading failures. An approach is proposed to analyze how the deployment and performance of thermal barriers in a battery pack determine their capabilities against cascading failures. The approach includes thermal propagation models associated with the simulations, degradation models, reliability analysis, and barrier analysis. Its application is illustrated with a practical case study. The battery reliabilities are sensitive to many factors of the barriers, such as temperature differences, failed cells, and performance coefficient. The barriers between parallel cells are found to be more effective in mitigating failure propagation. Such findings can be beneficial for barrier optimization and reliability improvement of battery packs.

## 1. Introduction

Lithium-ion batteries have been widely used as the principal power source in electric vehicles and other storage systems. They have attracted extensive interest due to their superior attributes, such as high energy density, lack of memory effect, long cycle life, and low self-discharge rates [1]. However, several critical issues still exist in lithium-ion batteries [2], e.g. risks related to battery performance and degradation [3,4]. Several accidents due to vehicle battery degradations have occurred, e.g., in the United States [5], Norway [6], Switzerland [1], and China [7]. It is desirable to continuously monitor and analyze battery performance to keep passangers of electric vehicles safe [8].

Reliability is always regarded as one of the most critical indicator of system performance [9], and battery reliability is reflected by lifecycle number, relating to many factors like temperature, discharge and charge, and C-rates [10]. Notably, temperature has a huge influence on battery reliability. Most commercial lithium-ion batteries operate efficiently, ranging from 20℃ to 40℃ [11]. However, the temperature of one cell may increase due to some failures, like overcharging, elevated internal resistance, crash, nail penetrations, melting the separator, decomposition of the cathode and electrolyte, and short-circuit [12,13]. Such a cell is thus failed, and the failure may cause thermal propagation to the surrounding cells by the heat transfer. Such thermal propagation is considered a cascading failure (CAF), which in general refers to the multiple failures initiated by a failed item resulting in a chain reaction [14].

Safety barriers can be installed in battery packs to eliminate the effects of CAFs [15]. Safety barriers are the physical or non-physical means to prevent, control, or mitigate undesired events [16], also called as countermeasures, defenses, mitigating measurements, and layers of protection [16]. In practices, several thermal safety barriers are needed to control CAFs [17], and the barrier performance, such as endothermic behavior, thermal resistance, material, arrangement, and temperature distribution path, may impact the mitigation effects [18].

The purpose of this paper is to investigate the mitigation effects of thermal barriers in lithium-ion battery packs. It is intended to study the impact of CAFs on battery reliability and analyze the layout of the thermal barriers, and to help designers to optimize the deployment of thermal barriers while keeping safety of batteries.

* Corresponding author.
*E-mail address:* yiliu.liu@ntnu.no (Y. Liu).

https://doi.org/10.1016/j.ress.2022.108804
Received 1 November 2021; Received in revised form 5 August 2022; Accepted 3 September 2022
Available online 5 September 2022

**Nomenclature**

| | |
|---|---|
| CAF | cascading failure |
| CFD | computational fluid dynamics |
| $T$ | temperature |
| $q$ | heat flux per time per area |
| $\rho$ | density |
| $q_{\mathrm{Q}}$ | heat generation rate |
| $I$ | charge/discharge current of cells |
| $R_{\mathrm{c}}$ | internal resistance of cells |
| $q_{\mathrm{c}}$ | heat flux for convection |
| $\mathrm{T_s}$ | surface temperature |
| $T_M$ /$T_W$ | temperatures at cell center/surface |
| $r$ | battery cell radius |
| $\varepsilon$ | emissivity |
| $\mathrm{T_1}$/ $\mathrm{T_2}$ | temperature of radiation surfaces |
| $\delta\xi$ | capacity degrading rate |
| R | gas constant |
| $\mathrm{SoC_{avg}}$ | average of SoC |
| $k_{si}$ | model parameters |
| Ah | amount of charge processed |
| $\Delta T_{\mathrm{nm}}$ | thermal propagation matrix |
| $\delta\xi_{ref}$ | capacity fading rate under reference condition |
| SoC | state of charge |
| SoH | state of health |
| $t$ | propagation time |
| $C_v$ | specific heat capacity |
| $\lambda$ | thermal conductivity |
| $V_c$ | volume of cell |
| $U$ | open-circuit voltage of cells |
| $\Delta T$ | temperature difference |
| $q_{\mathrm{r}}$ | heat flux for radiation |
| $\mathrm{T_a}$ | air temperature |
| $q_T$ | total heat flux from failed cell |
| $\mathrm{h_f}$ | convective heat transfer coefficient |
| $\sigma$ | Stefan-Boltzman constant |
| $W$ | given demand of SoH |
| $\theta$ | performance coefficient |
| $E_\alpha$ | activation energy |
| $\mathrm{SoC_{dev}}$ | normalized standard deviation |
| $N$ | charge/discharge lifecycle number |
| $\mathrm{R_{pack}}$ | reliability of the battery pack |
| $P_B$ | barrier function matrix |
| $\mathrm{Q_{max}}$ | maximum charges are drawn from the degraded and nominal batteries |

## 2. Related works and objectives

This section reviews the work related to reliability analysis and barrier analysis for lithium-ion batteries and formulates the research questions and objectives of this paper.

Performance of a cell or a battery pack can be indicated by its state of health (SoH), which is a variable that reflects the health condition of battery and represents the ability to deliver energy compared with the nominal state [19]. Normaly, when the SoH drops to 80% of the initial value, the cell or the battery pack is usually regarded to reach the end of lifetime [4]. In the following parts of this paper, when battery performance is mentioned, it is always based on SoH.

A large body of research has been devoted to modeling, analyzing and improving battery reliability. For example, impacts of degradation [20,21], configuration [22] and responses [20] on reliability of lithium-ion battery packs [22] been studied. Prediction of remaining lifes of lithium-ion batteries are conducted with physics-based models considering degradation mechanisms, like thermal disequilibrium [23–25] and degradation modes, such as discharge capacity and temperature [26], and time-varying temperature conditions [27]. Data-driven approaches, such as machine-learning techniques [21,28], Bayesian method [29], and the deep learning method [30], also have been involved in remaining life prediction. Wang et al. [27] have studied the influence of dependence among cells for the overall degradation of lithium-ion battery packs.

Some other researchers pay their attentions to the effects of CAFs in lithium-ion batteries, in consideration of materials properties, configuration, test environment, cathode chemistry, and electrical connectivity. For example, Lamb et al. have studied failure propagation in multi-cell lithium-ion batteries [31], with the findings that pouch cells propagate failures faster than cylindrical cells. Ouyang et al. [32] have investigated the impact of thermal failure propagation in various configurations: triangular, rectangular, parallelogram, linear, square, and hexagon. In [33], a series of thermal failure research has been conducted to explore the effects of failure propagations from many factors, such as gaps, state of charge (SoC), and phase change material. Yuan et al. [34] have considered the aging effect of the overcharge-induced thermal runaway of lithium-ion batteries. Coman et al. [35] have presented a numerical model for analyzing heat propagations in a battery pack.

Safety barriers in a battery pack have also been investigated to prevent CAFs. Such barriers can be battery thermal management systems, thermal barriers, gas vents, phase change materials, and fire extinguishing devices. For example, considering the thermally induced shutdown of lithium-ion batteries due to thermal propagation [36,37], one preventive approach is to use polymers as thermal barriers between cells [38]. Since a battery pack is actually a system consisting of cells connected in certain structure, it is interesting to know whether the deployment of thermal barriers are related to the structure, and how they can be layouted to be more effective in terms of mitigation of thermal propagation.

To obtain such knowledge, this paper is expected to: 1) investigate the effects of thermal barriers, as a CAF, on battery performance; 2) propose an approach for modeling thermal barriers against CAFs; 3) analyze how the deployment of the barriers impact their effectiveness against CAFs.

CAFs may lead to a thermal runaway or battery performance loss [15], and many researchers have studied the previous consequence while this paper will focus on the latter one. In our context, when the increased temperature of a cell is still in the operational range, and the battery pack can be used in degradation modes. The thermal propagation may be in a short time but occur in every cycle, then the degradation due to these CAFs last in long-time. Thus, the novelty of this paper lies investigation of such degradation and deployment approach of thermal barriers against CAFs. The expected results can help the designers optimize thermal barriers and improve battery reliability considering CAFs.

The rest of the paper is organized as follows. Section 3 presents a framework for modeling battery reliability considering CAFs. Then, in section 4, the models for thermal barriers in a battery pack are suggested. Moreover, an illustrative example is provided in section 5. Finally, we conclude and discuss future works in Section 6.

## 3. Performance analysis considering CAFs

This section presents a reliability and barrier analysis approach for a lithium-ion battery pack considering CAFs.

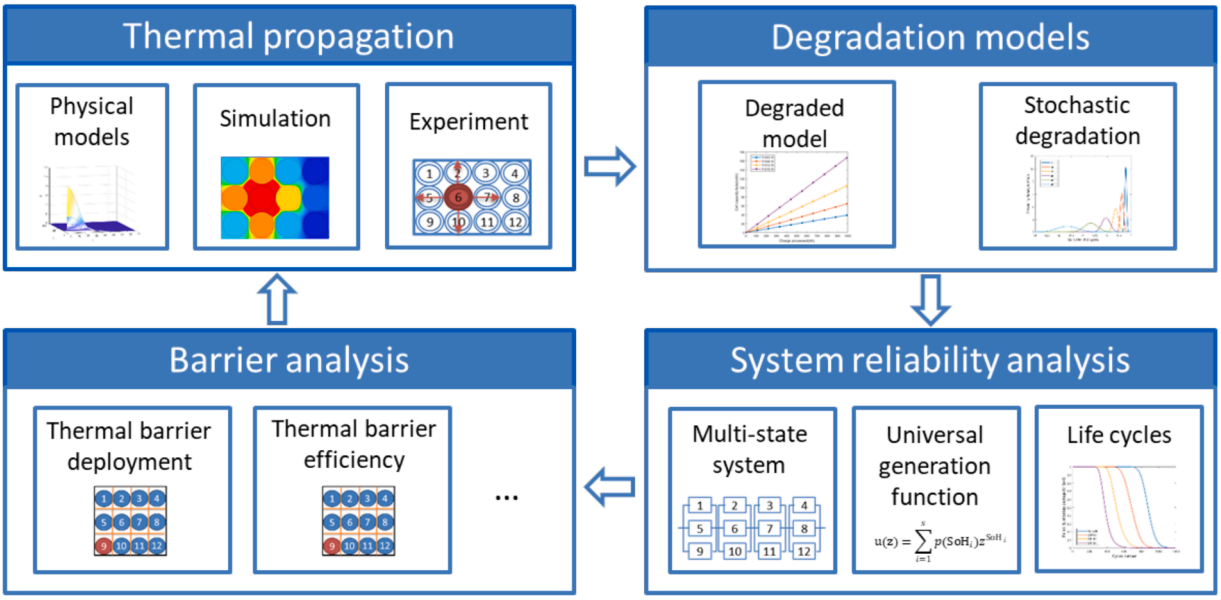


**Fig. 1.** The framework of reliability analysis and barrier analysis.

### 3.1. Framework of the analysis approach

The framework mainly includes four steps, as illustrated in Fig. 1. The first step is to analyze thermal propagation behaviors using thermal propagation models and simulations. Experiments can be used to verify the results.

The second step is to establish degradation models. The cell performance is degraded along with the increasing temperature. Individual cells are assumed to be degraded differently due to thermal propagations, material variation, manufacturing process, and damages during charge and discharge [22]. Therefore, stochastic degradation models are employed in this step.

The third step is related to performance analysis. Here, battery performance refers to the reliability of a battery pack, or the probability that it can fulfill the required function. A battery pack is regarded as a multi-state system with different degradations [39]. A universal generation function is applied to such a multi-state system to define the relationship between cells and packs, providing advanced and accurate results [21].

The last step is to analyze the effects of thermal barriers against CAFs. This paper mainly focused on the deployment and performance of thermal barriers.

### 3.2. Thermal propagation models

Three heat transfer models are usually used for thermal propagation: heat conduction, convection, and thermal radiation. Heat losses from thermal convection and thermal radiation can be negligible inside battery cells due to the poor fluidity of the electrolyte and low temperature [22]. The fundamental differential equation for heat conduction can generally obtain the temperature distribution. For uniaxial heat conduction, the governing equation can be written as:

$$\rho C_v \frac{\partial T}{\partial t} = \nabla(\lambda \nabla T) + q \tag{1}$$

where $\rho$ is the density ($kg\ m^{-3}$), $C_v$ is the specific heat capacity ($J\ kg^{-1}\ K^{-1}$), $T$ is the temperature ($K$), $q$ is the heat flux per time per area ($J\ m^{-2}\ s^{-1}$), and $\lambda$ is the thermal conductivity of the battery material ($W\ m^{-1}\ K^{-1}$). The battery cells are assumed to be homogeneous, although they are composed of different materials. The reason is that the electrode is thin, and reactions mainly occur between the electrode and electrolyte surface.

It has been concluded that the 2D model gives a slight temperature difference compared with the 3D model [35]. Thus, this paper uses the 2D model, and failed cell is regarded as a heat source. Then, the equivalent circuit model is commonly used to represent heat generations. The cell is equivalent to the internal resistance model with a resistor and voltage source series connection. Therefore, the heat generation rate due to a failed cell can be obtained in its simplified form as [22]:

$$q_Q = \frac{1}{V_c}\left[I^2 \mathrm{R}_C - IT\left(\frac{dU}{dT}\right)\right] \tag{2}$$

where $q_Q$ is heat generation rate ($W\ m^{-3}$), $V_c$ is the volume of the cell ($m^3$), $I$ is the charge and discharge current of the cell (A), $U$ is the open-circuit voltage of the cell ($V$), $\mathrm{R_c}$ is the internal resistance of the cell ($\Omega$). The thermal isolation on the surface of cells is ignorable if a large battery pack is considered. The maximum temperature reached at the center of the battery cell due to the heat generation rate can be estimated with the Eq. (3), derived from Fourier's law for long cylinder [40]:

$$\Delta T_{max} = T_M - T_W = \frac{q_Q r^2}{4\lambda} \tag{3}$$

where $T_M$ and $T_W$ are the temperatures at the battery cell center and on its surface, respectively ($K$), and $r$ is the battery cell radius ($m$). On the surface of the battery cells, thermal convection and thermal radiation should be considered [40]:

$$q_T = q_c + q_r \tag{4}$$

where $q_T$ is the total heat flux generated by the failed cell and absorbed by the surrounding battery cells ($W\ m^{-2}$), and $q_c$ and $q_r$ are the heat fluxes generated by convection and radiation ($W\ m^{-2}$) estimated with the Eqs. (5) and (6):

$$q_c = h_f[\mathrm{T}_s - \mathrm{T}_a] \tag{5}$$

$$q_r = \varepsilon\sigma\left[\mathrm{T}_1^4 - \mathrm{T}_2^4\right] \tag{6}$$

where $\mathrm{T_s}$ and $\mathrm{T_a}$ are the surface temperature, and air temperature ($K$), respectively, and $\varepsilon$ is the emissivity of the surface of the gray body. The emissivity is the effectiveness in emitting energy as thermal radial, which is assigned to be 1 for the perfect black body [22]. It is used to

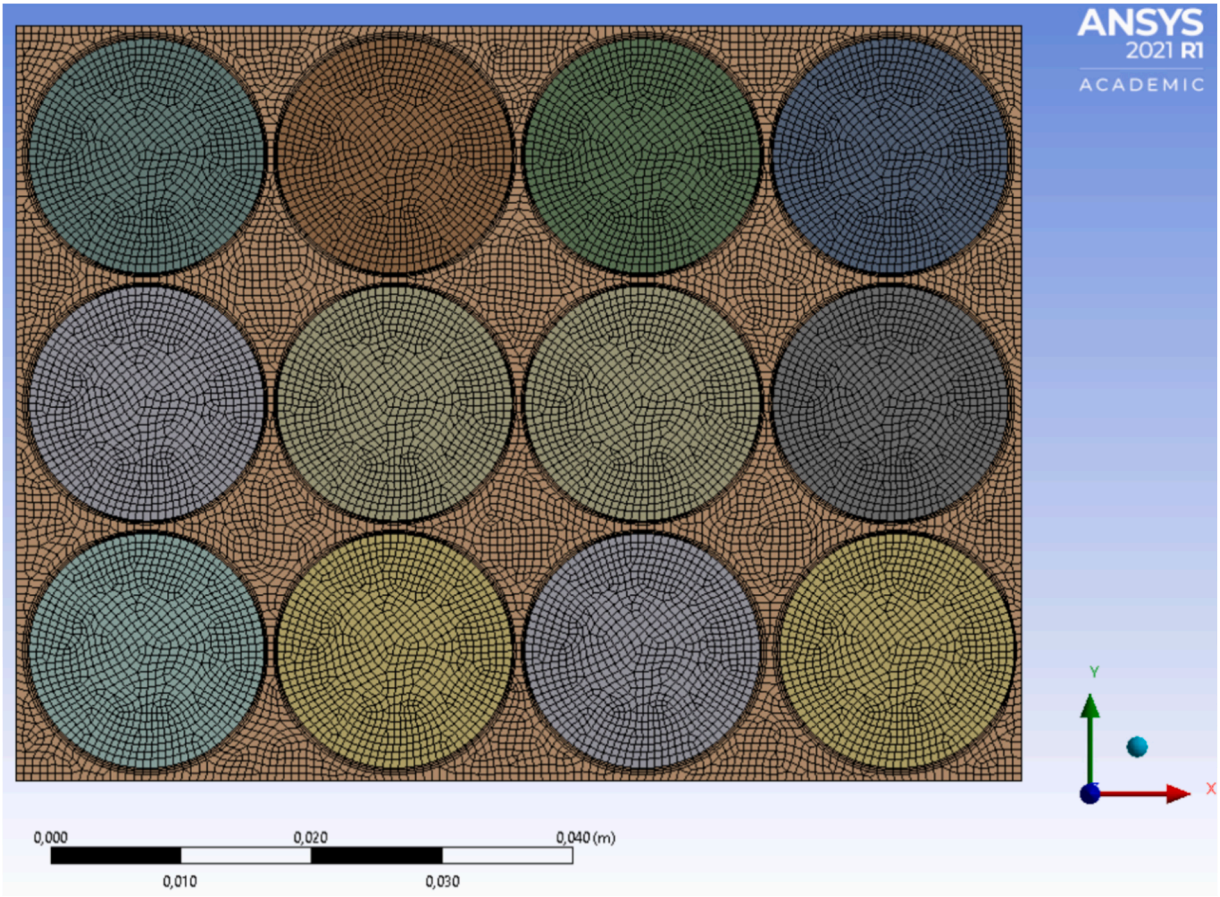


**Fig. 2.** Computational mesh employed in the thermal propagation analysis.

obtain the most conservative estimation for the thermal distribution. It was found to be a very slight decrease in the temperature estimation and cell degradation even if the value was changed from 1 to 0.9. $h_f$ is the convective heat transfer coefficient ($W\ m^{-2}\ K^{-1}$), σ is the Stefan-Boltzman constant ($5.67 \times 10^{-8}\ W\ m^{-2}\ K^{-1}$), and $T_1$ and $T_2$ are the temperatures of the two surfaces ($K$). The heat is assumed to be equally distributed to the battery cells with the same distance and orientation as the failed cell. The thermal propagation matrix, denoted by $\Delta T_{nm}$ for the cells ($C_{n\times m}$) in the battery pack, is therefore obtained as:

$$\Delta T_{nm} = \begin{bmatrix} \Delta T_{11} & \cdots & \Delta T_{1m} \\ \vdots & \ddots & \vdots \\ \Delta T_{n1} & \cdots & \Delta T_{nm} \end{bmatrix} \tag{7}$$

### 3.3. Thermal propagation simulation

Thermal analysis is conducted in ANSYS Fluent® to verify the results of the thermal propagation model described in Section 3.2. A 2D computational fluid dynamics (CFD) transient model is based on the cross-section area of a battery pack. The domain of the simulation is the battery box section with a rectangular shape. The battery pack is considered a closed adiabatic system without mass and heat transfer toward its surroundings. Therefore, this model sets the wall boundary condition for the battery pack containing the battery cells.

It should be noted that the thermal propagation during charging and discharging may be in a short time. However, the degradation due to these CAFs may last in long time cycles. The temperature at the surface of the failed cell is kept constant for the whole simulation duration, which is 10 minutes with a time step of 0.01 s. This simulation time is chosen long enough to observe the thermal effects of the failed cell on the surrounding cells but is limited to 10 minutes. This transient simulation is carried out in Fluent to understand time dependence on the thermal distribution of the cells surrounding the failed one. The parametric CFD model is more accurate than the analytical one. The simulated time can be varied to investigate how the distribution affects the surroundings. In addition, the CFD model can estimate the fluid behavior despite the cooling effect being neglected in this study. The computational grid reported in Fig. 2 had 16,631 elements with a minimum cell size of $6 \times 10^{-4}$ mm close to the battery surface. Then, the failed cell with increasing temperature can be set as a source of thermal propagations. Therefore, the thermal propagation matrix can be obtained based on the simulations.

### 3.4. Degradation model

The cells will be degraded during charging and discharging. The temperature dependence of the degrading capacity rate has been analyzed with the Arrhenius equation [9]:

$$\delta\xi(T) = \delta\xi_{ref}\exp\left[-\frac{E_a}{R}\left(\frac{1}{T}-\frac{1}{T_{ref}}\right)\right] \tag{8}$$

where $\delta\xi$ is the degrading capacity rate, $\delta\xi_{ref}$ is the capacity fading rate under the reference conditions, $R$ is the gas constant, $E_\alpha$ is the activation energy, and $T_{ref}$ is the reference temperature.

The capacity fading equation is linearly dependent on the charge processed, corresponding to the state of battery SoC [9]. Therefore, the empirical equation for capacity fading rate under the reference conditions is given as:

$$\delta\xi_{ref}\left(\mathrm{SoC}_{avg}, \mathrm{SoC}_{dev}\right) = k_{s1}\mathrm{SoC}_{dev}\exp\left(k_{s2}\mathrm{SoC}_{avg}\right) + k_{s3}\mathrm{SoC}_{dev}\exp\left(k_{s4}\mathrm{SoC}_{dev}\right) \tag{9}$$

where $SoC_{avg}$ is the average of SoC, and $SoC_{dev}$ is the normalized standard deviation from $SoC_{avg}$. $k_{s1}$, $k_{s2}$, $k_{s3}$, and $k_{s4}$ are model parameters and can be estimated from experiments. By combining Eqs. (5) and (6), the total degraded capacity is the summation of the degraded capacity under the experienced operating conditions and is calculated by:

$$\xi(T,\ SoC_{avg}, SoC_{dev}, Ah) = \left[k_{s1} SoC_{dev} \exp(k_{s2} SoC_{avg}) + k_{s3} SoC_{dev} \exp(k_{s4} SoC_{dev})\right] \cdot \exp\left[-\frac{E_a}{R}\left(\frac{1}{T} - \frac{1}{T_{ref}}\right)\right] \cdot N \cdot Ah \tag{10}$$

where $N$ represents the number of charge/discharge lifecycles, and $Ah$ is the amount of charge processed per charge/discharge. Then, the health state of cell SoH can be defined as [41]:

$$SoH = \frac{Q_{max}(\text{degraded})}{Q_{max}(\text{nominal})} = \left[1 - \frac{\xi}{Q_{max}(\text{nominal})}\right] \cdot 100\% \tag{11}$$

where $Q_{max}$(degraded) and $Q_{max}$(nominal) are the maximum charges drawn from the degraded and nominal batteries. Based on Eq. (11), we can obtain SoH for each cell during lifecycles.

### 3.5. System reliability model

A battery pack is considered a multi-state system with different degraded cells. If the number of cells in the battery pack is large, SoH is assumed to follow a normal distribution according to the central limit theorem [22]. The states of cells are classified into S groups based on the value of $SoH_i$ ($i$ =1,2, …, S). The u-function of the cells can be defined as [42]:

$$U_{(i,j)}(z) = \sum_{i=1}^{S} \sum_{j=1}^{S} p(SoH_i) p(SoH_j) z^{\otimes(SoH_i, SoH_j)} \tag{12}$$

where $p(SoH_i)$ is the probability at the state of $z^i$, $\otimes$ represents a composition operator over u-functions of cells connected in parallel or series. When cells are connected in series, the cell with the lowest $SoH_i$ becomes the bottleneck, and the SoH of the pack is equal to the minimum SoH. On the contrary, when cells are connected in parallel, the SoH of a pack is equal to the maximum SoH. If the SoH of a battery pack is less than a given demand $W$ ($W$ is typically defined as 80%), the battery pack is in a failed state. Therefore, the reliability of the battery pack is obtained as:

$$R_{pack} = P\left[U_{(i,j)}(z) \geq W\right] = \sum_{i=1}^{s} \sum_{j=1}^{s} p(SoH_i) p(SoH_j) \left[\otimes (SoH_i, SoH_j) \geq W\right] \tag{13}$$

If CAFs occur in a battery pack, the temperature of specific cells will be impacted, thereby influencing SoH. Therefore, the battery reliability for a battery pack can be calculated after CAF propagations based on SoH.

## 4. Modeling thermal barriers considering CAFs

This section is intended to model thermal barriers in a battery pack considering their deployment and performance.

### 4.1. Deployment of thermal barriers

A battery pack may include several thermal barriers. Thermal barriers can be physical and prevent CAFs from propagating to surrounding cells. Several deployment strategies, such as vertical, horizontal, and grid, may exist. A function matrix $P_B$ is introduced to represent the preventing ability of thermal barriers. For example, vertical thermal barriers are installed when cell $C_1$ initiates CAFs. The barrier function matrix $P_B$ can be defined as:

$$P_B = \begin{bmatrix} 1 & \cdots & 0 \\ \vdots & \ddots & \vdots \\ 0 & \cdots & 0 \end{bmatrix}$$

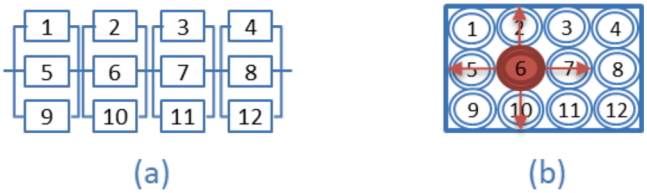


**Fig. 3.** different configurations of the battery pack.

**Table 1**
The values of the physical properties of battery cells [22].

| Parameter of cell | Parameter | Value |
|---|---|---|
| Dimension | Diameter (mm) | 18 |
| | Height (mm) | 65 |
| | Battery box (width × length, mm) | 58 × 77 |
| | Distance between cell surfaces (mm) | 1 |
| Electronic properties | Nominal voltage (V) | 3.2 |
| | Nominal capacity (Ah) | 1.1 |
| | Internal resistance (mΩ) | 30 |
| Thermal properties | Density ($kg\ m^{-3}$) | 2460.50 |
| | Specific heat capacity ($J\ kg^{-1}\ K^{-1}$) | 696.07 |
| | Thermal conductivity ($W\ m^{-1}K^{-1}$) | 67.20 (radial)/0.17 (axial) |

### 4.2. Performance of thermal barriers

A performance coefficient $\theta$ is introduced to describe barrier performance regarding the absorption ability. The performance coefficient depends on many factors, such as materials, thickness, and temperature behavior [43]. The thermal matrix after thermal propagation considering barrier performance can be obtained as:

$$\Delta T_{nm'} = \Delta T_{nm} P_B \theta \tag{15}$$

## 5. A case study of thermal barriers

This section conducts a case study to illustrate how to analyze the effects of CAFs and thermal barriers. In this paper, reliability analysis concerns failed cells and temperature differences, while barrier analysis concerns the deployment and performance of barriers. A battery pack consists of 12 cells structured as 3P4S, as illustrated in Fig. 3 (a). For example, Fig. 3 (b) shows that CAFs are initiated from the failed cell $C_6$, then CAFs are spread out.

### 5.1. Thermal propagations

Cylinder battery A123 APR 18650 with the capacity of 1.1 Ah is used in the analysis since they have been widely used. The physical properties of the battery pack are listed in Table 1. The charge/discharge rate is assumed to be 1C. The cells are assumed to have an initial SoC of 100% and cycled with a 100% depth of discharge. In addition, $SoC_{avg}$ and $SoC_{dev}$ are 50%. The parameters $k_{s1}$, $k_{s2}$, $k_{s3}$ and $k_{s4}$ are -4.09E-4, -2.17, 1.41E-5 and 6.13, respectively [9]. The gas constant is 8.31451, activation energy $E_\alpha$ is 78.06 ($kmol\ J^{-1}$), and the reference temperature $T_{ref}$ is 298.15 K.

The initial temperature for all cells is assumed to be the reference temperature of 25 ℃ (298.15 K). Then, thermal propagation matrixes can

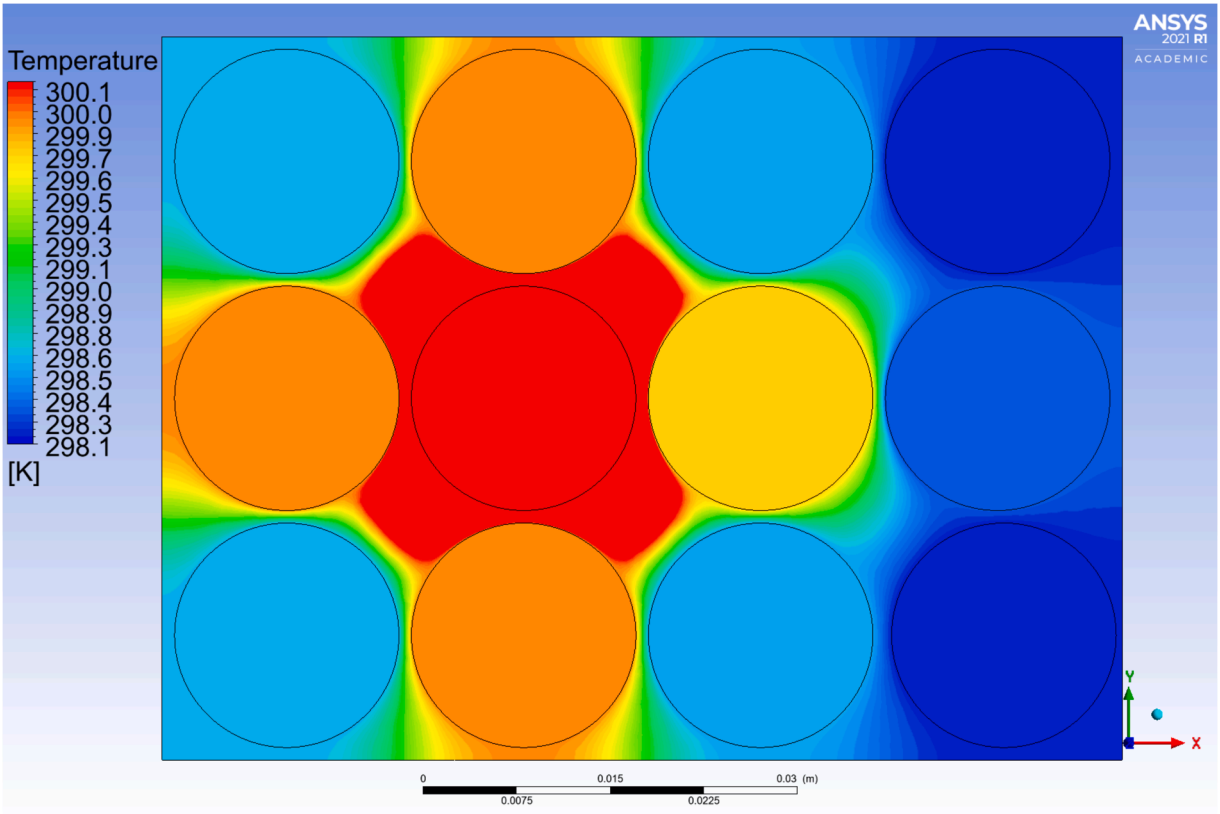


**Fig. 4.** Temperature of surrounding cells after propagations when C6 increases by 10°C.

be obtained based on Eqs. (1)-(7). For example, when the temperature on the surface of failed cell $C_6$ increases by 10C, the thermal propagation matrix is obtained as:

$$\Delta T_{nm}(\mathrm{C6}) = \begin{bmatrix} 0.55 & 1.66 & 0.55 & 0.05 \\ 1.66 & 17.65 & 1.66 & 0.14 \\ 0.55 & 1.66 & 0.55 & 0.05 \end{bmatrix}$$

The simulations are also conducted in Ansys Fluent® to verify the relevant results. Four failed cells (i.e., $C_1$, $C_2$, $C_3$, and $C_4$) and three temperature differences (i.e., 10/20/30°C) are considered in the stimulations. Only four positions are modeled by exploiting the double symmetry of the domain. The temperature and pressure of the battery box and its content (i.e., cells and air) are initially set to 25°C and 1.013 MPa, respectively. The effect of the cooling system is not considered.

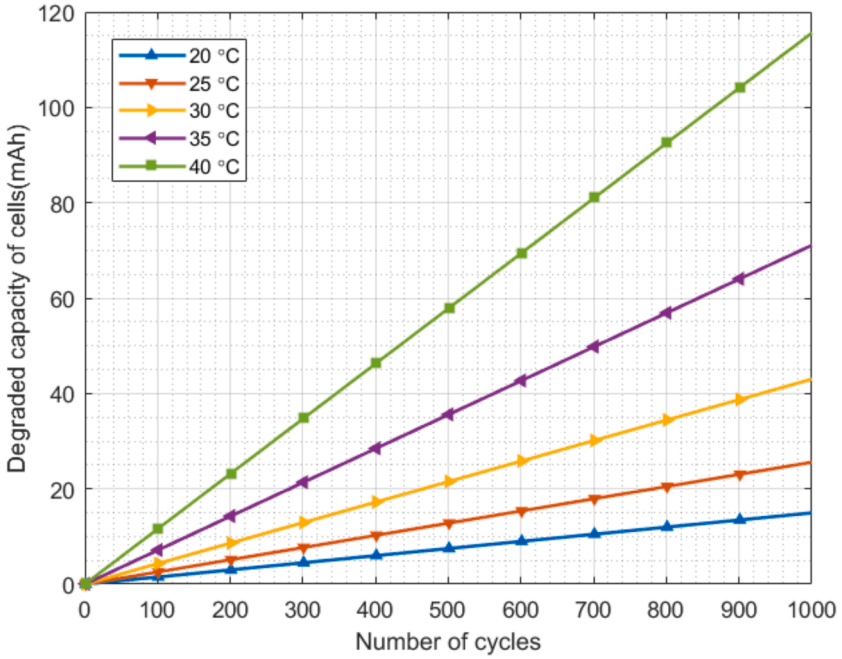


**Fig. 5.** Degraded capacity of battery cell under different temperatures.

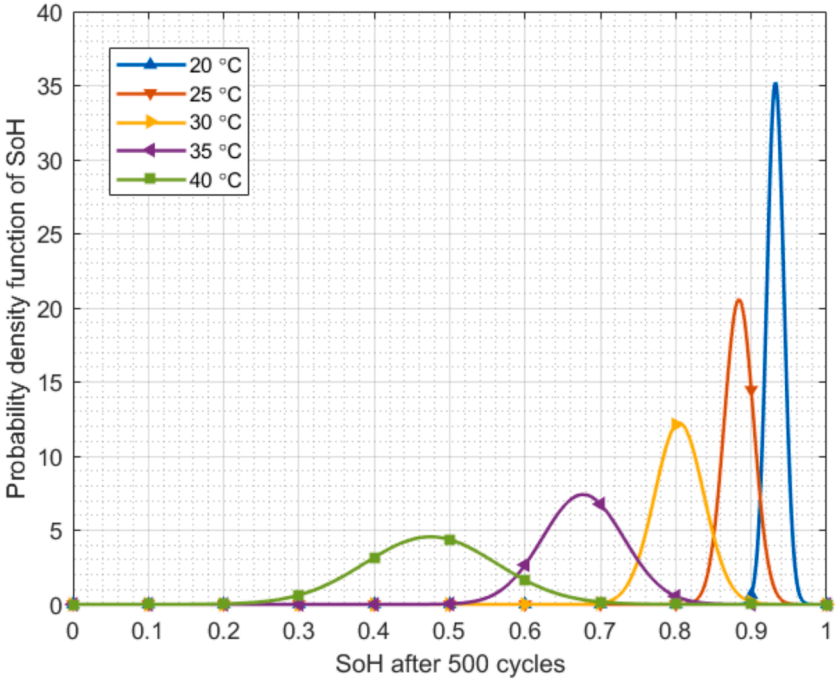


**Fig. 6.** Probability density function of SoH at different temperatures after 500 lifecycles.

Thus, the air is not moving in the domain. Therefore, a laminar viscous model is selected, and thermal propagation matrixes can be obtained from the simulations. For example, when the temperature of $C_6$ increases by 10℃, the temperature gradient inside $C_6$ and average surrounding temperature after CAF propagations are illustrated in Fig. 4.

The results from thermal propagation models give similar results as the simulations for all the cases (i.e., twelve simulations). For example, when the temperature of failed cell $C_6$ increases by 10℃, the thermal propagation matrix based on the average temperature can be obtained as:

$$\Delta T_{nm}(C6) = \begin{bmatrix} 0.47 & 1.77 & 0.41 & 0.06 \\ 1.77 & 13.56 & 1.61 & 0.18 \\ 0.47 & 1.77 & 0.42 & 0.05 \end{bmatrix}$$

The simulations are thus demonstrated to be suitable for simulating thermal propagations. In the following sections, therefore, we conduct the analysis based on the results of the simulations.

### 5.2. Degradation analysis

Based on Eqs. (10) and (11), one can obtain the capacity of battery cells depending on discharge/charge processed under different temperatures, as illustrated in Fig. 5. To calculate the battery reliability, SoH is assumed to be stochastically degraded. According to the central limit theorem, if the number of cells is large, SoH can be regarded as a normal distribution with $N(\mu, \sigma^2)$ [22]. Here, $\mu$ is the mean value of SoH of the battery cells, and SoH varies from [0,1]. Since three standard deviations in either direction cover roughly 99.7% of the data, the standard deviation $\sigma$ can thus be defined as (1- $\mu$)/6. Then, we can obtain the probability density function of SoH. Fig. 6 shows an example of the probability density function for SoH at different temperatures after 500 lifecycles.

### 5.3. Reliability analysis

U-function coefficient after different lifecycles can be obtained based on Eqs. (12) and (13). For example, Table 2 gives the coefficients of the U-function based on the thermal matrix. SoH is categorized into three groups: $SoH_1$<80%, 80%<$SoH_2$<90%, 90%< $SoH_3$<100%. When the given demand W is 80%, one can obtain battery reliability by adding the coefficient of $SoH_2$ and $SoH_3$. For example, the battery reliability is 0.9838 after 600 lifecycles.

**Table 2**
U-function coefficients after N lifecycle given temperature of $C_6$ increases by 10°;C.

| *N* | $SoH_1$ | $SoH_2$ | $SoH_3$ |
|---|---|---|---|
| 100 | 0.0000 | 0.0000 | 1.0000 |
| 200 | 0.0000 | 0.0000 | 1.0000 |
| 300 | 0.0000 | 0.0162 | 0.9838 |
| 400 | 0.0000 | 0.7069 | 0.2931 |
| 500 | 0.0000 | 0.9975 | 0.0025 |
| 600 | 0.0162 | 0.9838 | 0.0000 |
| 700 | 0.2272 | 0.7728 | 0.0000 |
| 800 | 0.7069 | 0.2931 | 0.0000 |
| 900 | 0.9608 | 0.0025 | 0.0000 |
| 1000 | 0.9975 | 0.0005 | 0.0000 |
| 1100 | 0.9999 | 0.0001 | 0.0000 |

Fig. 7 illustrates the battery reliability when the failed cell $C_6$ initiates CAFs. As seen, the battery reliability decreases along with an increasing temperature. That means CAFs have a significant impact on battery reliability.

It is natural to assume that the effects of CAFs initiated from failed cells may differ. Similarly, the calculations are performed for different failed cells (i.e., $C_1$, $C_2$, $C_5$, and $C_6$) when the temperatures of the surfaces increase by 30℃. As shown in Fig. 8, the battery reliabilities are sensitive to the failed cells. For example, the batteries are more reliable when $C_1$ and $C_2$ initiate CAFs. In addition, the reliability profile for $C_5$ is close to the one for $C_6$. Therefore, from the battery reliability perspective, $C_5$ and $C_6$ are more critical to be protected from CAFs.

The sensitivity analysis of temperature differences is also carried out. As shown in Fig. 9, when $C_6$ initiates CAFs, the influence from the temperature difference is more significant than that from $C_1$. The results emphasize that we should pay more attention to the temperatures of the cells $C_5$, $C_6$, $C_7$, and $C_8$. Therefore, the following sections focus on the case when $C_6$ initiates CAFs.

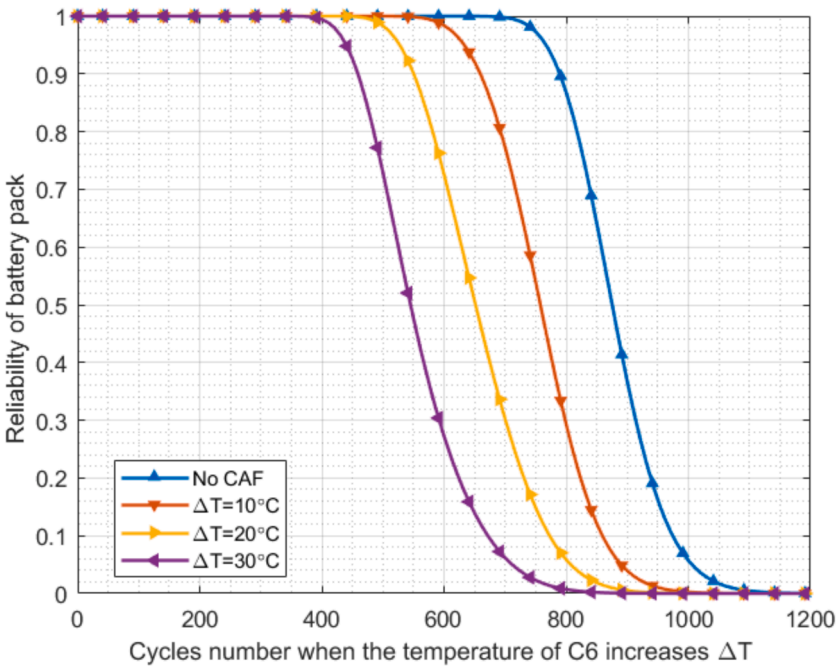


**Fig. 7.** Battery reliability given that $C_6$ initiates thermal CAFs.

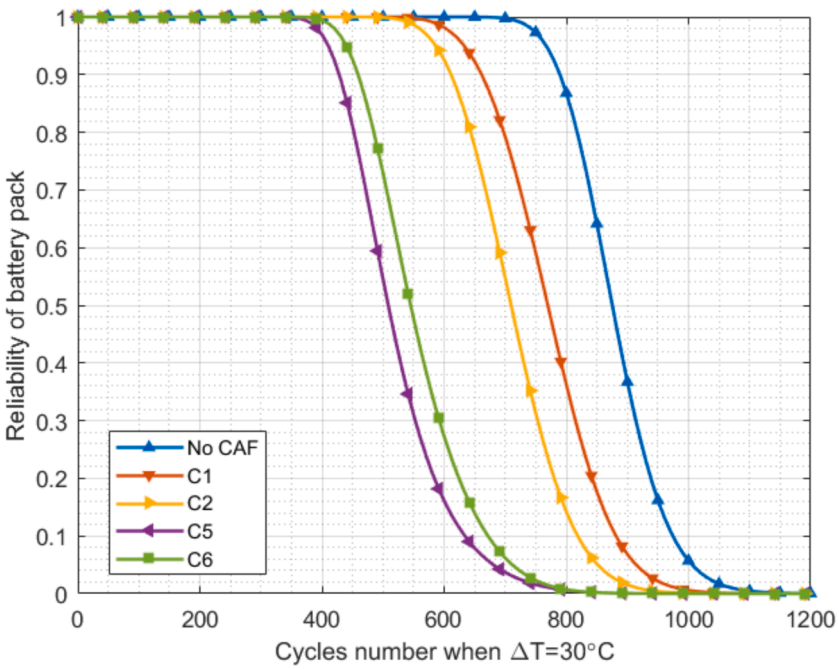


**Fig. 8.** Battery reliability for different initial failed cells.

### 5.4. Barrier analysis

This section considers thermal barriers against thermal CAFs. Fig. 10 shows the three types of deployment strategy: (a) vertical, (b) horizontal, and (c) grid.

First, consider perfect thermal barriers, meaning that thermal barriers can entirely prevent CAF propagations. For example, when the temperature of $C_6$ increases by 30℃, Fig. 11 illustrates the effects of different barrier strategies. The effects of the barriers in strategy (a) are more than those from strategy (b) in this case. In addition, the impact of the barriers in strategy (c) is close to that of strategy (b). This analysis can help the designers compare the barrier strategies with a limited budget.

Fig. 12 shows the battery reliability when the failed cell $C_6$ initiates CAFs. The reliability with the barriers in strategy (a) is sensitive to the temperature difference on $C_6$. However, the reliability profile with the barriers in strategy (b) is more stable. It can be concluded that, in this case, the effects of strategy (b) are superior to strategy (a), considering the mitigation effects. The horizontal barriers interrupt thermal propagation between the parallel cells in Fig. 13(a). Therefore, the barriers that stop the CAF propagations in parallel cells can be more efficient and effective in improving battery reliability.

When considering imperfect thermal barriers, it is required to introduce performance coefficient $\theta$ to express the preventing ability.

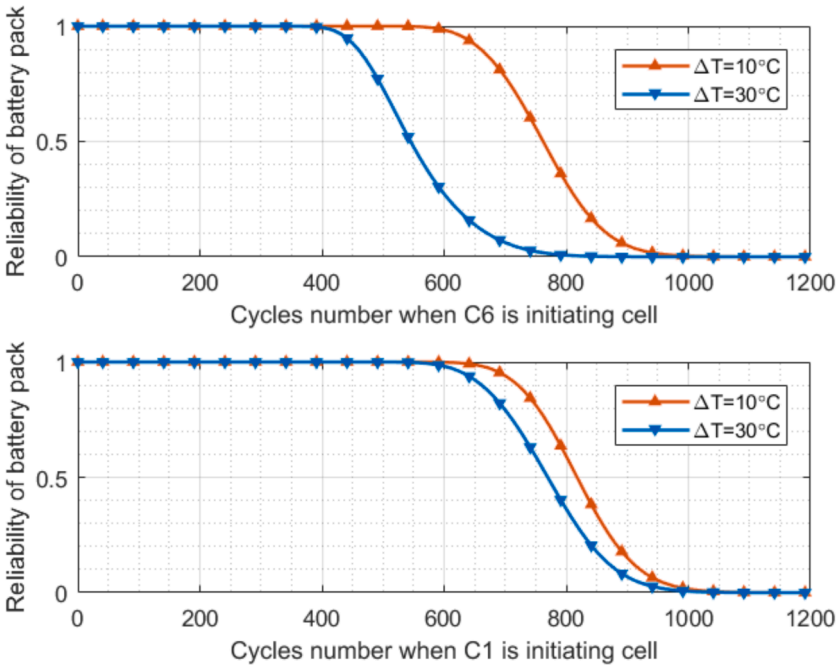


**Fig. 9.** Battery reliability considering temperature difference and initiating cells.

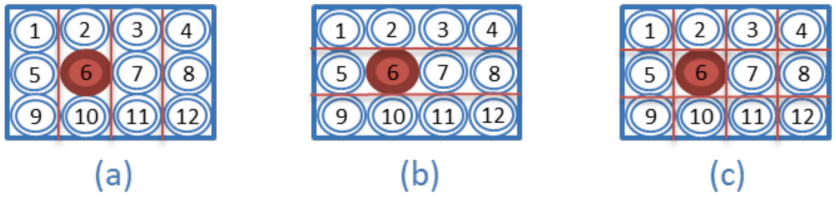


**Fig. 10.** Different thermal barrier strategies.

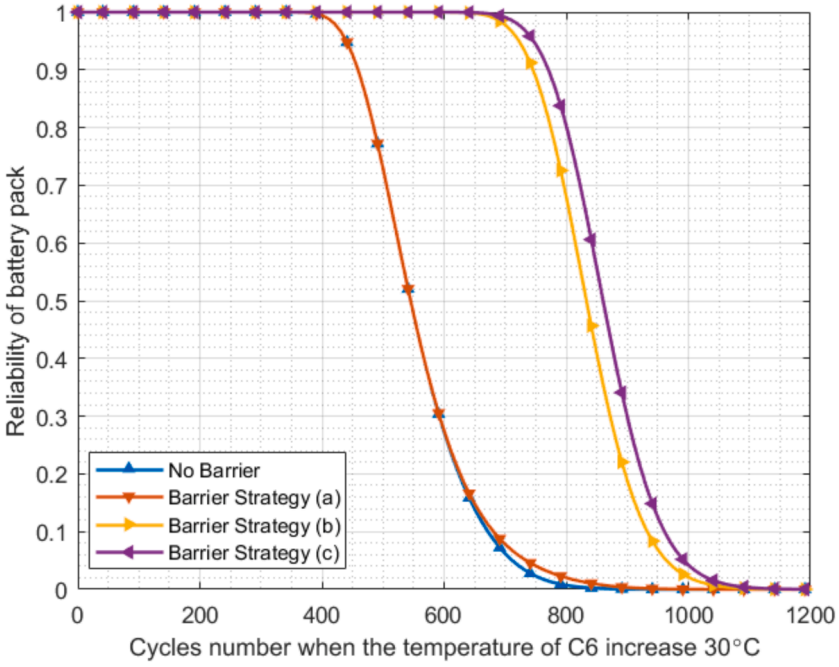


**Fig. 11.** Battery reliability for different barrier strategies.

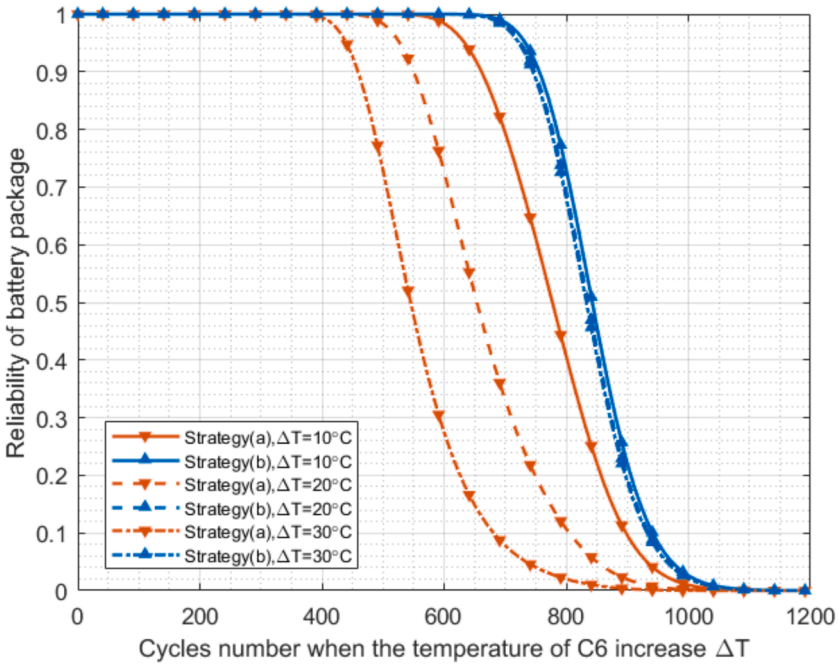


**Fig. 12.** Battery reliability with barriers considering temperature changes.

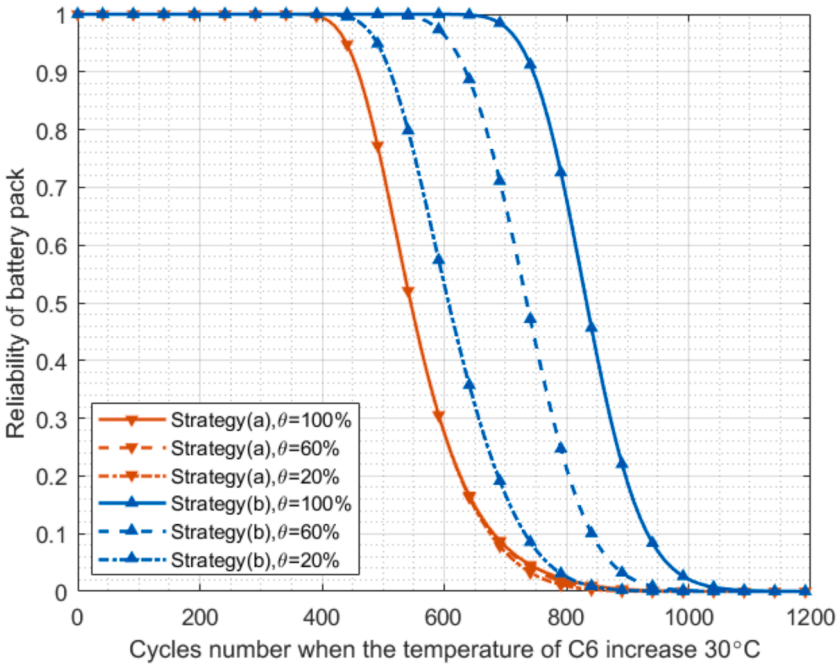


**Fig. 13.** Battery reliability considering the thermal barrier performance.

For example, in Fig. 3 when performance coefficient θ are 100%, 60%, and 20%, there exist apparent gaps between the reliability profiles and the strategy barriers (b). However, the reliability profiles for the strategy (a) barriers are the same regardless of the barrier performance. That implies that we need to consider the barrier performance differently when using different strategies. In addition, the cost of thermal barriers can also be considered in the analysis, and it can help the designers balance the effectiveness and the cost.

## 6. Conclusions and research perspectives

This paper focuses on the effects of thermal barriers in preventing CAFs in a battery pack. Table 3 summarizes the results obtained from the case study. It has been concluded that the battery reliabilities are sensitive to different factors of the barriers, such as temperature difference, location of the failed cell, and barrier coefficient. Generally, the barriers that disturb CAF propagations between the parallel cells more effectively improve battery reliability. Such information can help the designers optimize the deployment of thermal barriers and improve battery reliability.

Although the methods are promising for the reliability design, many factors are simplified and ignorable. For example, the internal resistance should be changed due to increasing temperature. In addition, other safety barriers, such as air cooling, gas vents, and battery thermal

**Table 3**
Summary of the results from analyzing thermal barriers.

| Battery reliability | Temperature difference | Location of failed cell | Thermal barrier performance coefficient |
|---|---|---|---|
| Battery with CAFs | √ | √ | - |
| Battery with CAFs and vertical barriers | √ | √ | × |
| Battery with CAFs and horizontal barriers | × | × | √ |
| Battery with CAFs and imperfect barriers | √ | √ | - |

Note: '√' represents sensitive, ' × ' represents non-sensitive

management system, have not been considered in this paper. Further, a battery cell is regarded as homogeneous. Therefore, it is necessary to carry out experiments to verify the proposed models. However, implementing experiments has several challenges, such as long-degraded time, high cost, and collaboration with industries.

The assumption of instantaneous prevention in this paper is somewhat limited. In practices, thermal propagations can be delayed by introducing barriers. Therefore, time-dependent models for the barrier performance can be considered, and the transient model to implement safety barriers can be developed in future studies. The study concerned only one typical configuration, but the conclusion should also be restrictive. Therefore, another research direction can investigate the effects of safety barriers in different cell arrangements and configurations. It is also interesting to perform further barrier analysis, e.g., multilevel barriers analysis.

## CRediT authorship contribution statement

**Lin Xie:** Conceptualization, Data curation, Investigation, Methodology, Writing – original draft, Writing – review & editing. **Federico Ustolin:** Methodology, Software, Validation, Visualization. **Mary Ann Lundteigen:** Conceptualization, Supervision, Writing – review & editing. **Tian Li:** Funding acquisition, Writing – review & editing. **Yiliu Liu:** Conceptualization, Supervision, Writing – review & editing, Project administration.

## Declaration of Competing Interest

The authors declare that they have no known competing financial interests or personal relationships that could have appeared to influence the work reported in this paper.

## Data availability

Data will be made available on request.

## Acknowledgments

This research is with the support from the Fire Research and Innovation Centre (FRIC) funded by the Research Council of Norway (No. 294649). We also appreciate the anonymous reviewers for their comments.

## References

[1] Chombo PV, Laoonual Y. A review of safety strategies of a Li-ion battery. J Power Sources 2020;478:228649.
[2] Liu W, Tobias P, Chau KT. Overview of batteries and battery management for electric vehicles. Energy Rep 2022;8:4058–84.
[3] Tarascon J-M, Armand M. Issues and challenges facing rechargeable lithium batteries. Materials for sustainable energy: a collection of peer-reviewed research and review articles from Nature Publishing Group. 2011. p. 171–9.
[4] Han X, Lu L, Zheng Y, Feng X, Li Z, Li J, et al. A review on the key issues of the lithium ion battery degradation among the whole life cycle. ETransportation 2019; 1:100005.
[5] Beauregard GP. Report of investigation: Hybrids plus plug in hybrid electric vehicle. US Department of Energy, Idaho National Laboratory; 2008.
[6] Feng X, Ouyang M, Liu X, Lu L, Xia Y, He X. Thermal runaway mechanism of lithium ion battery for electric vehicles: a review. Energy Storage Mater 2018;10: 246–67.
[7] Wang Q, Mao B, Stoliarov SI, Sun J. A review of lithium ion battery failure mechanisms and fire prevention strategies. Prog Energy Combust Sci 2019;73: 95–131.
[8] Tang T, Yuan H. A hybrid approach based on decomposition algorithm and neural network for remaining useful life prediction of lithium-ion battery. Reliab Eng Syst Saf 2022;217:108082.
[9] Rausand M, Hoyland A. System reliability theory: models, statistical methods, and applications. John Wiley & Sons; 2003.
[10] Lam L, Bauer P. Practical capacity fading model for Li-ion battery cells in electric vehicles. IEEE Trans Power Electron 2012;28:5910–8.
[11] Gandoman FH, Jaguemont J, Goutam S, Gopalakrishnan R, Firouz Y, Kalogiannis T, et al. Concept of reliability and safety assessment of lithium-ion batteries in electric vehicles: Basics, progress, and challenges. Appl Energy 2019; 251:113343.
[12] Becher D, Bauer M, Döring H, Böse O, Friess B, Danzer MA. Preventing thermal propagation in battery packs using enthalpy supported thermal barriers. J Energy Storage 2021;42:103057.
[13] Spotnitz R, Franklin J. Abuse behavior of high-power, lithium-ion cells. J Power Sources 2003;113:81–100.
[14] Xie L, Lundteigen MA, Liu YL. Reliability and barrier assessment of series–parallel systems subject to cascading failures. In: 234. Proc Inst Mech Eng Part O J Risk Reliab; 2020. p. 455–69.
[15] Zhang J, Zhang L, Sun F, Wang Z. An overview on thermal safety issues of lithium-ion batteries for electric vehicle application. IEEE Access 2018;6:23848–63.
[16] Sklet S. Safety barriers: definition, classification, and performance. J Loss Prev Process Ind 2006;19:494–506.
[17] Lee C, Said AO, Stoliarov SI. Passive mitigation of thermal runaway propagation in dense 18650 lithium ion cell assemblies. J Electrochem Soc 2020;167:090524.
[18] Etacheri V, Marom R, Elazari R, Salitra G, Aurbach D. Challenges in the development of advanced Li-ion batteries: a review. Energy Environ Sci 2011;4: 3243–62.
[19] Xia Q, Yang DZ, Wang ZL, Ren Y, Sun B, Feng Q, et al. Multiphysical modeling for life analysis of lithium-ion battery pack in electric vehicles. Renew Sustain Energy Rev 2020;131:109993.
[20] Xia Q, Wang ZL, Ren Y, Tao LF, Chen L, Tian J, Hu DZ, et al. A modified reliability model for lithium-ion battery packs based on the stochastic capacity degradation and dynamic response impedance. J Power Sources 2019;423:40–51.
[21] Li C, Chen X, Yi X. Reliability analysis of primary battery packs based on the universal generating function method. In: 223. Proc Inst Mech Eng Part O J Risk Reliab; 2009. p. 251–7.
[22] Liu Z, Tan C, Leng F. A reliability-based design concept for lithium-ion battery pack in electric vehicles. Reliab Eng Syst Saf 2015;134:169–77.
[23] Xia Q, Wang Z, Ren Y, Sun B, Yang D, Feng Q. A reliability design method for a lithium-ion battery pack considering the thermal disequilibrium in electric vehicles. J Power Sources 2018;386:10–20.
[24] Downey A, Lui Y-H, Hu C, Laflamme S, Hu S. Physics-based prognostics of lithium-ion battery using non-linear least squares with dynamic bounds. Reliab Eng Syst Saf 2019;182:1–12.
[25] Xu F, Yang F, Fei Z, Huang Z, Tsui K-L. Life prediction of lithium-ion batteries based on stacked denoising autoencoders. Reliab Eng Syst Saf 2021;208:107396.
[26] Mishra M, Martinsson J, Rantatalo M, Goebel K. Bayesian hierarchical model-based prognostics for lithium-ion batteries. Reliab Eng Syst Saf 2018;172:25–35.
[27] Wang L, Sun Y, Wang X, Wang Z, Zhao X. Reliability modeling method for lithium-ion battery packs considering the dependency of cell degradations based on a regression model and copulas. Materials 2019;12:1054.
[28] He J, Tian Y, Wu L. A hybrid data-driven method for rapid prediction of lithium-ion battery capacity. Reliab Eng Syst Saf 2022;226:108674.
[29] Ardeshiri RR, Ming L, Chengbin M. Multivariate stacked bidirectional long short term memory for lithium-ion battery health management. Reliab Eng Syst Saf 2022;224:108481.
[30] Xu X, Tang S, Yu C, Xie J, Han X, Ouyang M. Remaining useful life prediction of lithium-ion batteries based on wiener process under time-varying temperature condition. Reliab Eng Syst Saf 2021;214:107675.
[31] Lamb J, Orendorff CJ, Steele LAM, Spangler SW. Failure propagation in multi-cell lithium ion batteries. J Power Sources 2015;283:517–23.
[32] Ouyang D, Liu J, Chen M, Weng J, Wang J. Thermal failure propagation in lithium-ion battery modules with various shapes. Appl Sci 2018;8:1263.
[33] Ouyang D, Weng J, Hu J, Chen M, Huang Q, Wang J. Experimental investigation of thermal failure propagation in typical lithium-ion battery modules. Thermochim Acta 2019;676:205–13.
[34] Yuan W, Liang D, Chu Y, Wang Q. Aging effect delays overcharge-induced thermal runaway of lithium-ion batteries. J Loss Prev Process Ind 2022;104830.
[35] Coman PT, Darcy EC, Veje CT, White RE. Numerical analysis of heat propagation in a battery pack using a novel technology for triggering thermal runaway. Appl Energy 2017;203:189–200.

[36] Torres-Castro L, Kurzawski A, Hewson J, Lamb J. Passive mitigation of cascading propagation in multi-cell lithium ion batteries. J Electrochem Soc 2020;167:090515.
[37] Baginska M, Blaiszik BJ, Merriman RJ, Sottos NR, Moore JS, White SR. Autonomic shutdown of lithium-ion batteries using thermoresponsive microspheres. Adv Energy Mater 2012;2:583–90.
[38] Zhou Z, Zhou X, Wang B, Liew KM, Yang L. Experimentally exploring thermal runaway propagation and prevention in the prismatic lithium-ion battery with different connections. Process Saf Environ Prot 2022;164:517–27.
[39] Levitin G, Xing L. Reliability and performance of multi-state systems with propagated failures having selective effect. Reliab Eng Syst Saf 2010;95:655–61.
[40] Cengel Y, Ghajar A. Heat and mass transfer: fundamentals and applications. Singapore: McGraw-Hill Education; 2021.
[41] Ng KS, Moo C-S, Chen Y-P, Hsieh Y-C. Enhanced coulomb counting method for estimating state-of-charge and state-of-health of lithium-ion batteries. Appl Energy 2009;86:1506–11.
[42] Lisnianski A, Levitin G. Multi-state system reliability: assessment, optimization and applications. World scientific; 2003.
[43] Chen C, Reniers G, Khakzad N. A thorough classification and discussion of approaches for modeling and managing domino effects in the process industries. Saf Sci 2020;125:104618.